

See discussions, stats, and author profiles for this publication at: <https://www.researchgate.net/publication/41418284>

Ternary Lipid Bilayers Containing Cholesterol in a High Curvature Silica Xerogel Environment

ARTICLE *in* LANGMUIR · FEBRUARY 2010

Impact Factor: 4.46 · DOI: 10.1021/la9046885 · Source: PubMed

CITATIONS

13

READS

15

2 AUTHORS, INCLUDING:



Marjorie L Longo

University of California, Davis

115 PUBLICATIONS 3,405 CITATIONS

SEE PROFILE

Ternary Lipid Bilayers Containing Cholesterol in a High Curvature Silica Xerogel Environment

Emel I. Goksu and Marjorie L. Longo*

Department of Chemical Engineering & Materials Science, University of California, Davis, California 95616

Received December 12, 2009. Revised Manuscript Received January 18, 2010

The phase behavior of 1,2-dioleoyl-*sn*-glycero-3-phosphocholine (DOPC)/1,2-distearoyl-*sn*-glycero-3-phosphocholine (DSPC) (1/1 mol ratio)/cholesterol (0–60 mol %) supported lipid bilayers agreed with a DOPC/DSPC/cholesterol ternary phase diagram by Zhao et al. when a mica support was used (Zhao, J.; Wu, J.; Heberle, F. A.; Mills, T. T.; Klawitter, P.; Huang, G.; Costanza, G.; Feigenson, G. W. *Biochim. Biophys. Acta, Biomembr.* **2007**, *1768*, 2764–2776). However, when a silica xerogel support was used, the phase behavior deviated from the phase diagram. Specifically, miscibility and trend lines of DSPC-rich domain area fraction, domain shape, and domain size versus cholesterol, obtained by analysis of fluorescence and atomic force microscopy (AFM) images, were as expected for mica-supported lipid bilayers, but were substantially stretched to higher cholesterol concentrations for silica xerogel-supported lipid bilayers. In addition, this behavior was found in three other ternary lipid compositions substituting slightly shorter acyl chain lengths in comparison to DSPC or a saturated lipid versus unsaturated DOPC. Qualitative comparison of domain characteristics of DOPC/DSPC/cholesterol (0 and 15 mol %) bilayers supported by silica xerogel, mica, borosilicate glass, and quartz showed that the networked surface layer of high curvature (0.04 nm^{-1}) silica beads was the dominant influence as opposed to the surface chemistry. Based upon the literature, we postulate two curvature-based mechanisms that explain our results. In the first mechanism, cholesterol was transferred from the higher curvature supported lipid bilayer to the lower curvature vesicles in the medium during the vesicle fusion and thermal cooling step, resulting in a lowered cholesterol concentration of the supported lipid bilayer. In the second mechanism, high curvature promoted sustained lipid demixing as the cholesterol concentration was increased, thus creating a new phase diagram in which coexisting phases persist to a higher cholesterol concentration. These results suggest that a surface layer of high curvature features can be used to observe and study curvature-induced intrabilayer transport or demixing over large areas and that curvature can play an important role in sorting and localization of biomembrane components.

Introduction

The cell membrane is a two-dimensional fluid structure that can curve in three dimensions. Some examples of curved biomembranes are the vesicles by which chemicals are transported within and between cells, protrusions that provide cell motility and many unicellular organisms that have various shapes such as rods, spirals, and spheres.¹ In recent studies, the curvature within lipid bilayers, as models of cell membranes, was shown to be capable of playing an important role in lipid sorting² and localization.³ Studies relating curvature to lipid bilayer properties at different scales have been summarized by the authors and co-workers as part of a recent review.⁴

Silica xerogels have been demonstrated to be suitable substrates for single (egg phosphatidylcholine (PC))^{5,6} and two-phase (1,2-dioleoyl-*sn*-glycero-3-phosphocholine (DOPC)/1,2-distearoyl-*sn*-glycero-3-phosphocholine (DSPC))⁷ bilayers, providing a porous network structure beneath the lipid bilayers. We have shown by

atomic force microscopy (AFM) and quantitative fluorescence imaging techniques that the lipid bilayer on a silica xerogel continuously follows the surface corrugations and approximately covers the upper hemisphere of silica beads of the xerogel structure.⁷ Using spin-coating during the silica xerogel synthesis procedure, we could reliably produce silica xerogel substrates containing a surface layer of $\sim 50\text{ nm}$ ($1/r = 0.04\text{ nm}^{-1}$ curvature) beads. Such nanometer-scale curvature has been shown to alter transmembrane transport and lipid mixing in model membrane systems that employed small vesicles,^{8–10} individual coated beads,¹¹ or vesicle tethers² of nanometer-scale radius. The silica xerogel system is a particularly good candidate to observe and study these phenomena by fluorescence microscopy techniques and AFM imaging because it provides a substrate in which a high curvature environment persists over many square millimeters.

A large number of studies directed at the cell membrane have provided evidence for the existence of lipid and protein heterogeneities which are integrally involved with various cell functions such as trafficking of proteins and lipids,¹² cell signaling,¹³ protein sorting,¹⁴ and activation of immune responses.¹⁵ These

*To whom correspondence should be addressed. E-mail: mllongo@ucdavis.edu.

- (1) Parthasarathy, R.; Groves, J. T. *Soft Matter* **2007**, *3*, 24–33.
- (2) Tian, A.; Baumgart, T. *Biophys. J.* **2009**, *96*, 2676–2688.
- (3) Parthasarathy, R.; Yu, C. H.; Groves, J. T. *Langmuir* **2006**, *22*, 5095–5099.
- (4) Goksu, E. I.; Hoopes, M. L.; Nellis, B. A.; Xing, C.; Faller, R.; Frank, C. W.; Risbud, S. H.; Satcher, J. H.; Longo, M. L. *Biochim. Biophys. Acta, Biomembr.*, published online September 18, 2009, <http://dx.doi.org/10.1016/j.bbamem.2009.09.007>.
- (5) Weng, K. C.; Stalgren, J. J. R.; Duval, D. J.; Risbud, S. H.; Frank, C. W. *Langmuir* **2004**, *20*, 7232–7239.
- (6) Weng, K. C.; Stalgren, J. J. R.; Risbud, S. H.; Frank, C. W. *J. Non-Cryst. Solids* **2004**, *350*, 46–53.
- (7) Goksu, E. I.; Nellis, B. A.; Lin, W. C.; Satcher, J. H.; Groves, J. T.; Risbud, S. H.; Longo, M. L. *Langmuir* **2009**, *25*, 3713–3717.

- (8) McLean, L. R.; Phillips, M. C. *Biochim. Biophys. Acta* **1984**, *776*, 21–26.
- (9) Fugler, L.; Clejan, S.; Bittman, R. *J. Biol. Chem.* **1985**, *260*, 4098–4102.
- (10) Thomas, P. D.; Poznansky, M. J. *Biochem. J.* **1988**, *254*, 155–160.
- (11) Brumm, T.; Jorgensen, K.; Mouritsen, O. G.; Bayerl, T. M. *Biophys. J.* **1996**, *70*, 1373–1379.
- (12) Devaux, P. F. *Biochemistry* **1991**, *30*, 1163–1173.
- (13) Helms, J. B.; Zurzolo, C. *Traffic* **2004**, *5*, 247–254.
- (14) Keller, P.; Toomre, D.; Diaz, E.; White, J.; Simons, K. *Nat. Cell Biol.* **2001**, *3*, 140–149.
- (15) Langlet, C.; Bernard, A. M.; Drevot, P.; He, H. T. *Curr. Opin. Immunol.* **2000**, *12*, 250–255.

nanodomains, so-called “rafts”, are hypothesized to be rich in cholesterol (chol) which has a tremendous impact on the mechanical, crystalline packing, and mixing behavior of lipid mixtures.^{16,17} Rafts are believed to be in a liquid-ordered (L_o) phase^{18,19} in which the lipids have high lateral mobility as in the fluid (L_a) phase, but their acyl chains are extended and ordered as in the gel (L_β) phase.²⁰ Typically ternary mixtures that are used to study/model the fundamental properties of cell membranes, including the L_o domains of lipid rafts, contain cholesterol and two lipid components that in their pure forms form a fluid and gel phase lipid bilayer. Ternary phase diagrams determined for these mixtures at various temperatures have recently been compiled by Marsh.²¹ Characterizing changes in the phase behavior of such ternary mixtures induced by high curvature environments will be critical to understanding intramembrane and intermembrane transport and sorting in cells.

Here we characterize DOPC-rich domains in DOPC/DSPC (1/1 mol ratio)/chol (0–60 mol %) ternary mixtures supported on high curvature silica xerogel surfaces versus flat/smooth mica surfaces. We chose this ternary mixture because a full phase diagram (Figure 1) was available for comparison, determined by Zhao et al. using low curvature giant unilamellar vesicles (GUVs).²² Quantitative characterization of domain area fraction, domain shape factor, and domain size is carried out using analysis of fluorescence microscopy and AFM images. The role of surface curvature versus surface chemistry is examined by using substrates varying in surface chemistry and curvature. Finally, silica-xerogel- and mica-supported lipid bilayers made from three different ternary mixtures are examined (for one mixture quantitatively) to determine if the results obtained for the DOPC/DSPC/chol system could be generalized. Two different testable mechanisms, based upon the literature, are proposed for the quantitative differences in domain characteristics for smooth mica-supported versus high curvature silica xerogel-supported lipid bilayers. These mechanisms have implications in intrabilayer and interbilayer partitioning/sorting of membrane components.

Materials and Methods

Synthesis of the Silica Xerogel Thin Film Supports. A one-step base catalyzed sol–gel synthesis procedure was used to form the silica xerogel. A total of 8.6 g of tetramethoxysilane (TMOS, Acros Organics, Morris Plains, NJ) was mixed with 15.1 g of methanol (ACS Reagent, Sigma-Aldrich, Milwaukee, WI) for 15 min. In a separate beaker, 3.05 g of water, 15.1 g of methanol, and 100 μ L of a 28–30% NH₃ basic aqueous ammonium hydroxide (Sigma-Aldrich, Milwaukee, WI) solution were mixed for 15 min. The two mixtures were then combined such that the molar ratio for TMOS/H₂O/MeOH/NH₄OH was 1:3:16.7:0.01. This resulted in a gelling time of approximately 35 min. At approximately 10 min into the gelation process, 600 μ L of the gelling solution was pipetted onto a mica sample on a spin-coater (Chemat Technology Inc., Northridge, CA) with a speed of 3000 rpm and allowed to gel for 10 s. The samples were then transferred from the spin-coater to a sample holder where each was exposed to methanol vapor until the vesicle solution was deposited.

(16) Ohvo-Rekila, H.; Ramstedt, B.; Leppimaki, P.; Slotte, J. P. *Prog. Lipid Res.* **2002**, *41*, 66–97.

(17) Ramstedt, B.; Slotte, J. P. *FEBS Lett.* **2002**, *531*, 33–37.

(18) Brown, D. A.; London, E. *J. Biol. Chem.* **2000**, *275*, 17221–17224.

(19) Silvius, J. R.; delGiudice, D.; Lafleur, M. *Biochemistry* **1996**, *35*, 15198–15208.

(20) Ipsen, J. H.; Karlstrom, G.; Mouritsen, O. G.; Wennerstrom, H.; Zuckermann, M. J. *Biochim. Biophys. Acta* **1987**, *905*, 162–172.

(21) Marsh, D. *Biochim. Biophys. Acta, Biomembr.* **2009**, *1788*, 2114–2123.

(22) Zhao, J.; Wu, J.; Heberle, F. A.; Mills, T. T.; Klawitter, P.; Huang, G.; Costanza, G.; Feigenson, G. W. *Biochim. Biophys. Acta, Biomembr.* **2007**, *1768*, 2764–2776.

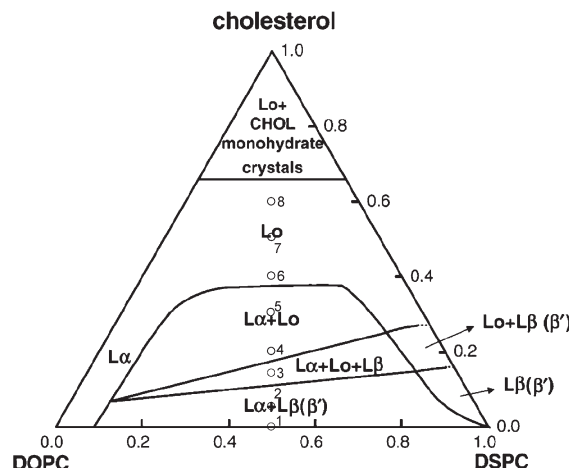


Figure 1. Ternary phase diagram for DOPC/DSPC/chol lipid bilayer from GUVs at 23 °C. The points in the center of the diagram (1–8) correspond to the experimental compositions of vesicles that were used to form supported lipid bilayers in this study (0, 5, 15, 20, 30, 40, 50, and 60 mol % chol in 1/1 mol ratio DOPC/DSPC). Reprinted from ref 22 with permission from Elsevier. Numbers (1–8) have been added.

Supported Lipid Bilayer Formation. DOPC, DSPC, 1,2-dipalmitoyl-sn-glycero-3-phosphocholine (DPPC), 1,2-dipenta-decanoyl-sn-glycero-3-phosphocholine (DiC15PC), 1,2-dilauroyl-sn-glycero-3-phosphocholine (DLPC), cholesterol (chol), and 1-palmitoyl-2-[6-(7-nitro-2-1,3-benzodiazol-4-yl)amino]hexanoyl-sn-glycero-3-phosphocholine (NBD-PC) were purchased from Avanti Polar Lipids (Alabaster, AL). A 1/1/0.005 mol ratio of (DOPC or DLPC)/(DSPC, DiC15PC, or DPPC)/NBD-PC and required amount of chol were mixed from chloroform solutions in glass reaction vials and dried under a stream of nitrogen. Lipids were then resuspended in nanopure water with a resistivity of ~18 MΩ cm (for mica- and silica xerogel-supported lipid bilayers) or in 5 mM sodium phosphate buffer (for glass- and quartz-supported lipid bilayers) to 1 mg/mL total lipid concentration. The solutions were held in a water bath at 65 °C for 5 min. After heating, the solutions were sonicated with a tip sonicator (Branson Sonifier, model 250, Branson Ultrasonics, Danbury, CT) for 1 min to obtain small unilamellar vesicles. A 250 μ L droplet of each solution was then pipetted onto freshly cleaved mica (prod. no. 52, Ted Pella, Inc., Redding, CA), borosilicate glass (Corning Labware, Corning, NY, Cover Glass #1, sonicated in detergent solution and water, respectively), quartz (SPI Supplies, West Chester, PA, Quartz Coverslip Thickness #0, sonicated in detergent solution and water, respectively), and silica xerogel substrates. After 5 min to allow vesicle fusion to take place, each sample was placed in ~15 mL of 65 °C water in a Petri dish in a temperature-controlled oven (Echotherm Chilling Incubator, model IN35, Torrey Pines Scientific, San Marcos, CA) and incubated at 65 °C for 30 min. The system was then cooled to room temperature with a programmed cooling rate. The samples were placed in nanopure water at room temperature, and excess vesicles were removed by rinsing, yielding “clean” supported lipid bilayers.

The supported lipid bilayers and substrates were scanned at room temperature with a Digital Instruments Dimension 3100 atomic force microscope (Santa Barbara, CA) equipped with Nanoscope software. Fluorescence imaging of lipid bilayers was carried out with a Nikon Eclipse 400 fluorescence microscope (Nikon, Melville, NY) equipped with a fluorescence filter cube (EF-4 FITC HYQ, Nikon) which matches to the excitation and emission spectrum of NBD-PC at room temperature. Images were captured by using an Orca digital camera (Hamamatsu, Japan). Image analysis was performed using ImageJ (National Institutes of Health, Bethesda, MD). The images were first subdivided into

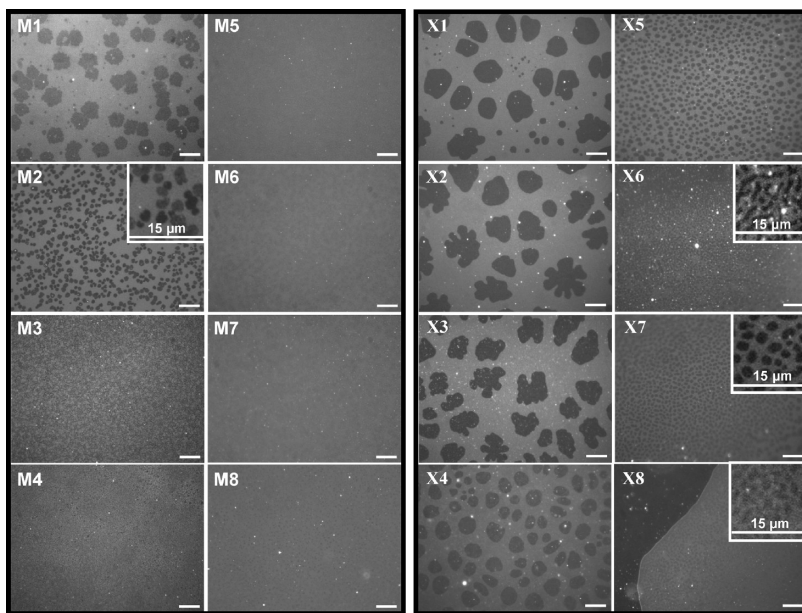


Figure 2. Fluorescence microscopy images of DOPC/DSPC/chol bilayers supported by mica (M1–8 on left, 10 °C/h cooling rate) and silica xerogel (X1–8 on right, 20 °C/h cooling rate) substrates formed from vesicles of the compositions given in Figure 1. Domain sizes are decreased more effectively by the addition of chol on the mica surface compared to the silica xerogel surface. Domains on silica xerogel persist through 60 mol % chol (X8) in disagreement with Figure 1, inferring a difference in composition and/or phase diagram on this high curvature/roughness surface. Scale bars represent 15 μ m.

smaller regions, and then the domain analyses were done by adjusting the threshold values for the domain detection followed by the “Analyze Particles” command. The domains at the edges were excluded in the shape factor and size analysis. The out-of-focus portions of some fluorescence images were not included in the analysis.

Results

Domain Characteristics of Mica- and Silica Xerogel-Supported DOPC/DSPC/Chol Bilayers. We prepared lipid bilayers supported by mica and silica xerogel by fusion of small unilamellar vesicles (SUVs) composed of 1/1 mol ratio DOPC/DSPC and increasing cholesterol (chol) mol % as shown on the phase diagram in Figure 1 as points 1–8 (0, 5, 15, 20, 30, 40, 50, and 60 mol % chol). In order to form similar sized DSPC-rich domains ($\sim 10 \mu\text{m}$ in diameter) at the starting composition (0 mol % chol), the mica-supported lipid bilayers were cooled from 65 to 23 °C at a rate of 10 °C/h and the silica xerogel-supported lipid bilayers were cooled at a faster rate of 20 °C/h. As shown in Figures 2 and 3, we imaged domains on mica at compositions 1–8 (M1–8) using fluorescence microscopy and AFM contact mode, respectively. As shown in Figures 2 and 3, we imaged domains on silica xerogel at compositions 1–8 (X1–8) using fluorescence microscopy and compositions 1–4 (X1–4) using AFM contact mode. AFM imaging was not used for samples X5–8 because the surface roughness is of similar magnitude to the height of the DSPC-rich domains above the DOPC-rich phase as shown in the AFM section analysis of Figure 3 (compare section analysis of M4 to X4), making AFM imaging increasingly difficult as the chol mol % is increased, whereby the height decreases further and domain fluidity is increased. All imaging in this study was performed at 23 °C. As it is evident from Figure 2 (M1–4), there was a dramatic decrease in the domain size on mica with the addition of chol, and domains are so small that they are not observable by fluorescence microscopy above 15 mol % chol (Figure 2, M3). Therefore, we also utilized AFM images, as will be presented below. Interestingly, at 5 mol % chol, bimodal

fluorescence intensities of the domains were observed (inset in M2, Figure 2). This cannot be attributed to the coexistence of symmetric (spanning both leaflets) and asymmetric (spanning one leaflet) domains because in AFM images the height difference between all domains and the surrounding fluid region is constant, (data not shown) and in fluorescence images, after the background subtraction, the fluorescence intensity of the lighter domains is not half that of the DOPC-rich areas (data not shown). Therefore, this is an indication of the three phase coexistence ($L_\alpha + L_\beta + L_\beta$) region in Figure 1.²³ We expect the darker domains to be the gel phase, L_β , domains as they strongly exclude the fluorescent dye²⁴ and the lighter domains to be liquid ordered, L_α , domains in a background of bright DOPC-rich liquid, L_α , phase.

As it is evident from Figure 2 (X1–4), domain sizes on silica xerogel did not substantially decrease with the addition of up to 20 mol % chol. As Figure 2 (X5–8) shows, domains substantially decreased in size beginning at 30 mol % chol but remained barely resolvable even at 60 mol % chol in fluorescent images (inset in X8, Figure 2). The presence of phase separated domains at 50 and 60 mol % chol does not agree with the ternary phase diagram of Figure 1 where at points 7 and 8 the mixture is in one single L_α phase. Importantly, by comparing X5 to M2 in Figure 2, it can be seen that the domain size at 30 mol % chol on silica xerogel resembles the domain size at 5 mol % chol on mica.

AFM is a higher resolution technique compared to standard fluorescence imaging and provides a more detailed investigation of the domains. Domains on mica could be observed in AFM images up to 40 mol % chol (point 6 in the phase diagram of Figure 1) as shown in Figure 3 (M1–6) but not at 50 mol % chol (M7). The mixture is in the L_α phase at 50 mol % chol according to Figure 1. Therefore, the miscibility point of the ternary lipid mixture on mica is approximately 40 mol % chol, in agreement with the phase diagram in Figure 1.

(23) Feigenson, G. W. *Biochim. Biophys. Acta, Biomembr.* **2009**, 1788, 47–52.
(24) Veatch, S. L.; Keller, S. L. *Biophys. J.* **2003**, 85, 3074–3083.

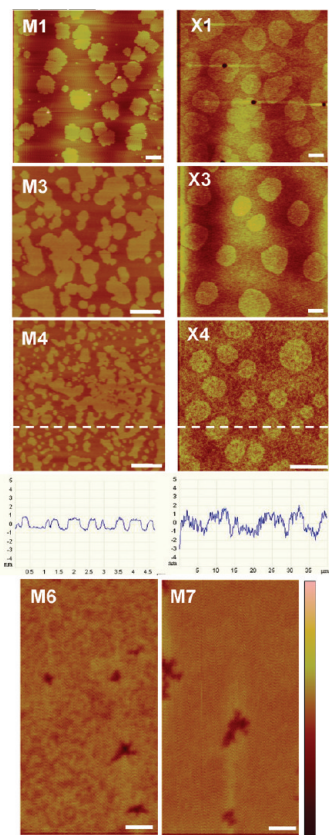


Figure 3. AFM high resolution images of DOPC/DSPC/chol bilayers supported by mica (M1, M3, M4, M6, and M7, 10 °C/h cooling rate) and silica xerogel (X1, X3, and X4, 20 °C/h cooling rate) substrates formed from vesicles of the compositions given in Figure 1. Submicrometer-scale domains on mica persist through 40 mol % chol (M6) but not 50 mol % chol (M7), in general agreement with Figure 1, and these domains are frequently merged (coalesced). Each lipid bilayer is significantly rougher on silica xerogel versus mica substrates by comparing images and section analysis of M4 and X4 (dotted lines and corresponding graphs). Scale bars represent 1 μm for M3, M4, M6, and M7 and 10 μm for the others. Color bar on the right represents 5 nm for M6 and M7 and 10 nm for the others.

The area fraction, shape, and size of the domains on mica become much more apparent by examining the AFM images. It is seen in Figure 3 that M1 (0 mol % chol) domains have a slightly leafy shape and the micrometer-sized M3 (15 mol % chol) domains appear to be merging (coalescing) and taking on a networked appearance that was barely discernible in the fluorescence microscope. The M4 (20 mol % chol) and M6 (40 mol % chol) domains were submicrometer and 100 nm in their narrow dimension, respectively, and thus, these were not visible in the fluorescence microscope. In addition, for M4, the area fraction of the domains had substantially increased in comparison to M1 (0 mol % chol) as seen in Figure 3. The domain area fractions of images M1 and M4 images are 0.34 and 0.48, respectively. For the silica xerogel-supported samples, Figure 3 (X1–4 and section analysis of X4) reveals that the lipid bilayer, including domains, follows the roughness of the substrate, in agreement with our previous work that only examined DOPC/DSPC (0 mol % chol).⁷ In addition, the size of the domains on silica xerogel did not decrease substantially at 20 mol % chol (Figure 3 X4) compared to 0 mol % chol (Figure 3 X1), in agreement with our fluorescence imaging; that is, there were no submicroscopic domains that were not visible by fluorescence microscopy.

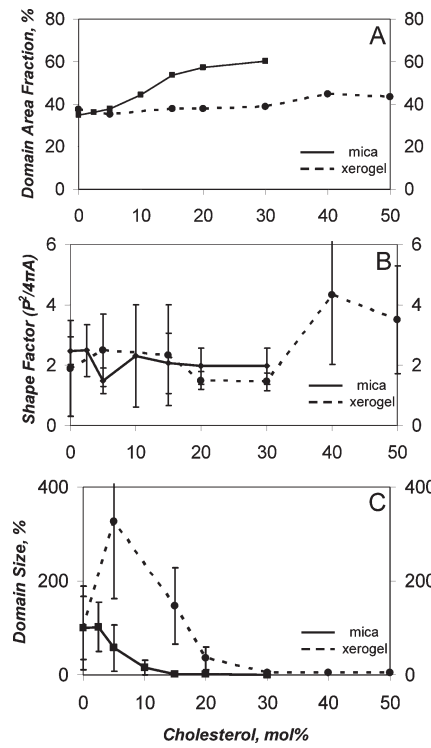


Figure 4. DOPC/DPSC (1/1 mol ratio)/chol bilayers supported by mica (solid lines) and silica xerogel (dashed lines) characterized for (A) domain area fraction, (B) shape factor, and (C) domain size versus chol concentration of vesicles used for supported lipid bilayer preparation (cooling rate of 20 °C/h). The domain area fraction is given in percent. The domain sizes are given in terms of % values with respect to 0 mol % chol results. Error bars represent one standard deviation. No error bars are present for domain area fraction, since the data were obtained using all images for each substrate.

We quantitatively characterized the DSPC-rich domains at increasing chol concentrations in Figure 4, in terms of domain area fraction, shape factor ($S = P^2/4\pi A$, where P is the perimeter and A is the area of the domains), and domain size (a percentage that is relative to the average domain area at 0 mol % chol). For this analysis, we used uniform thermal sample preparation conditions by cooling both mica-supported and silica xerogel-supported lipid bilayers from 65 to 23 °C at an identical rate (20 °C/h). Domains on mica were imaged by AFM, while the domains on silica xerogel were imaged by fluorescence microscopy.

The domain area fractions at increasing chol concentrations as shown in Figure 4A are useful for this investigation because each value is directly determined by the composition and phase diagram of the supported lipid bilayer according to the lever rule. Therefore, we can determine if the composition and/or phase behavior of each supported lipid bilayer is in agreement with the phase diagram of Figure 1 at the composition of the SUVs used to form the supported lipid bilayers. As shown in Figure 4A, the experimentally determined domain area fractions at 0 mol % chol are nearly identical for mica-supported and silica xerogel-supported lipid bilayers (0.35 and 0.38, respectively). These area fractions are in good agreement with the area fraction, 0.35, that we calculate using the lever rule applied to the 0 mol % tie line of Figure 1 at point 1 and assuming area per lipid values of 72.5 and 47.3 \AA^2 for DOPC²⁵ and DSPC²⁶ in fluid and gel phases,

(25) Petracche, H. I.; Tristram-Nagle, S.; Gawrisch, K.; Harries, D.; Parsegian, V. A.; Nagle, J. F. *Biophys. J.* **2004**, *86*, 1574–1586.

(26) Tristramnagle, S.; Zhang, R.; Suter, R. M.; Worthington, C. R.; Sun, W. J.; Nagle, J. F. *Biophys. J.* **1993**, *64*, 1097–1109.

respectively. This agreement implies that, at 0 mol % chol, the composition and phase behavior of the lipid bilayer on mica and silica xerogel are in good agreement with the composition of the vesicles used to prepare the lipid bilayers and the phase diagram of Figure 1. For this calculation, the fluidus boundary (left-hand boundary of the $L_\alpha+L_\beta$ region) was ~0.09 molar fraction of DSPC and the solidus boundary (right-hand boundary of the $L_\alpha+L_\beta$ region) was the pure DSPC vertex. This calculation assumed the DSPC domains were symmetrically distributed in agreement with the average height difference, ~1.8 nm, between the domains and surrounding fluid region on the mica substrate and fluorescence intensity measurements previously made for the silica xerogel substrate⁷ between the domains and surrounding fluid regions.

The domain area fraction on mica increased substantially upon the addition of chol as shown in Figure 4A. At 20 mol % chol, the domain area fraction had increased to 0.57. To calculate the expected area fraction based on vesicle composition, we use the property that the 20 mol % chol composition (point 4 in Figure 1) is in close proximity to the tie line that defines the upper boundary for the three-phase coexistence region and assume a parallel tie line. Application of the lever rule and assumption of identical area per molecule values for L_o and L_α phases results in an area fraction of 0.59. This agreement implies that, at 20 mol % chol, the composition of the lipid bilayer on mica is in good agreement with the composition of the vesicles used to prepare the lipid bilayers (1/1 mol ratio DOPC/DSPC 20 mol % chol) and the phase behavior is in agreement with the phase diagram in Figure 1.

On the other hand, on silica xerogel, the area fraction of the domains remained almost constant, as shown in Figure 4A, upon the addition of up to 30 mol % chol (~0.38). Importantly, the domain area fraction at 40 mol % chol increased to 0.45 which is very close to the mica results at 10 mol % chol, that is, 0.44. These results imply that, above 0 mol % chol, the composition and/or phase behavior of the lipid bilayers on the silica xerogel substrate may not be in agreement with the composition of the vesicles used to prepare the lipid bilayers and/or the phase diagram of Figure 1, respectively.

Domain shape was used as an indication of domain fluidity and phase. Domain shapes were quantified in Figure 4B by shape factor: circular, $S \sim 1$; leaflike, $S \sim 2$; and fractal, $S \sim 4.5$. These S values correspond to three different regimes of growth for crystalline domains, respectively: reaction limited, reaction+diffusion limited, and diffusion limited.²⁷ Gel phase domains at 0 mol % chol samples (point 1 in Figure 1) for both mica- and silica xerogel-supported lipid bilayers have S values ~2, meaning that they grew in the reaction+diffusion limited region. As the chol concentration within the domains increased, the domains became more fluidized and rounder, leading to lower S . At 5 mol % chol on mica, S decreased below 2. After this concentration, however, even though individual domains were rounded, there was an increase in S values as shown in Figure 4B due to merging (coalescence) of portions of neighboring domains (e.g., M3 in Figure 3). These changes in S occurred at significantly higher chol concentrations for silica xerogel-supported lipid bilayers, as shown in Figure 4B, where the decrease in S took place at ~20–30 mol % chol followed by an increase with further addition of chol.

The domain sizes in Figure 4C were given in terms of percentages with respect to the average of the domain area values

at 0 mol % chol. After addition of 2.5 and 15 mol % chol, the average domain size dropped below 100% for mica- and silica xerogel-supported lipid bilayers, respectively. Interestingly, the average domain size on silica xerogel at 5 mol % chol was approximately 3.5 times larger compared to the average domain sized at 0 mol % chol, which we will relate to Ostwald ripening in the Discussion. The domain sizes reached near 0% at 15 and 30 mol % chol for mica- and silica xerogel-supported lipid bilayers, respectively. In summary, the observed trend lines in domain area fraction, S , and domain size are substantially stretched to higher chol concentration for ternary lipid bilayers on silica xerogel compared to mica substrates.

Domain Characteristics: The Influence of Surface Chemistry versus Surface Curvature. There are substantial differences between mica and silica xerogel substrates in surface curvature/roughness and surface chemistry. In order to investigate separately the roles of curvature/roughness and surface chemistry in the observed trends, we compared visually the domain sizes of 0 and 15 mol % chol lipid bilayers on mica, silica xerogel, borosilicate glass, and quartz. Mica, borosilicate glass, and quartz are surfaces that are both flat and smooth with similar root-mean-square roughness values (0.15, 0.23, and 0.16 nm, respectively) as measured from AFM images like those on the left of Figure 5. On the other hand, as shown on the left of Figure 5, silica xerogel is made of interconnected beads with a diameter of 50 ± 21 nm in our synthesis conditions⁷ and a root-mean-square surface roughness value of 0.73 nm representing the roughness of the bead surfaces. Muscovite mica has a chemical composition of $KAl_2(Si_3Al)O_{10}(OH,F)_2$ with ~46 mol % SiO_2 . Borosilicate glass has more SiO_2 in its composition, 64 mol % SiO_2 . Quartz and silica xerogel are both composed of 100 mol % SiO_2 . Different cooling rates were used for each substrate (ranging from 5 to 20 °C/h) in this comparison in order to obtain similar sized domains for the 0 mol % chol conditions for this fluorescence microscopy observation. As shown in Figure 5, for the flat/smooth substrates of varying composition (borosilicate glass, quartz, and mica), the domain size decreased similarly from 0 to 15 mol % chol, by about an order of magnitude. In contrast, for the substrate of higher curvature/roughness (silica xerogel) and the same composition as quartz, the domain size remained approximately the same from 0 to 15 mol % chol as shown in Figure 5. This observation indicates that it is the surface curvature/roughness of silica xerogel, rather than the surface chemistry, that initiated the stretching of the domain area fraction, S , and domain size trend lines to higher mol % chol as shown in Figure 4.

Domain Characteristics: Generalization for Ternary Mixtures. In order to determine if the chosen lipid chain length or degree of unsaturation was an important determinant of the characteristic trends shown in Figure 4, we exchanged the gel phase lipid, DSPC (C18), for two shorter chain lipids, DPPC (C16) and DiC15PC (C15), and then we exchanged the doubly unsaturated fluid lipid, DOPC, for a saturated fluid lipid, DLPC. We prepared DOPC/DPPC/chol (Figure 6), DOPC/DiC15PC/chol (not shown), and DLPC/DSPC/chol (Figure 7) lipid bilayers with 1/1 mol ratio fluid lipid/gel lipid at increasing chol concentrations on mica and silica xerogel surfaces. All of the supported lipid bilayers were cooled from 65 to 23 °C with the identical cooling rate of 20 °C/h. Similar to our results for DOPC/DSPC bilayers, we observed that domain size is reduced more effectively by addition of chol when the mica substrate is used in comparison to the silica xerogel substrate. This trend can be seen by comparing domain sizes in the left panels and right panels of Figures 6 and 7. Also similarly, as shown in Figure 7 (silica xerogel 30%), domains were readily observable on silica xerogel for the

(27) Blanchette, C. D.; Orme, C. A.; Ratto, T. V.; Longo, M. L. *Langmuir* 2008, 24, 1219–1224.

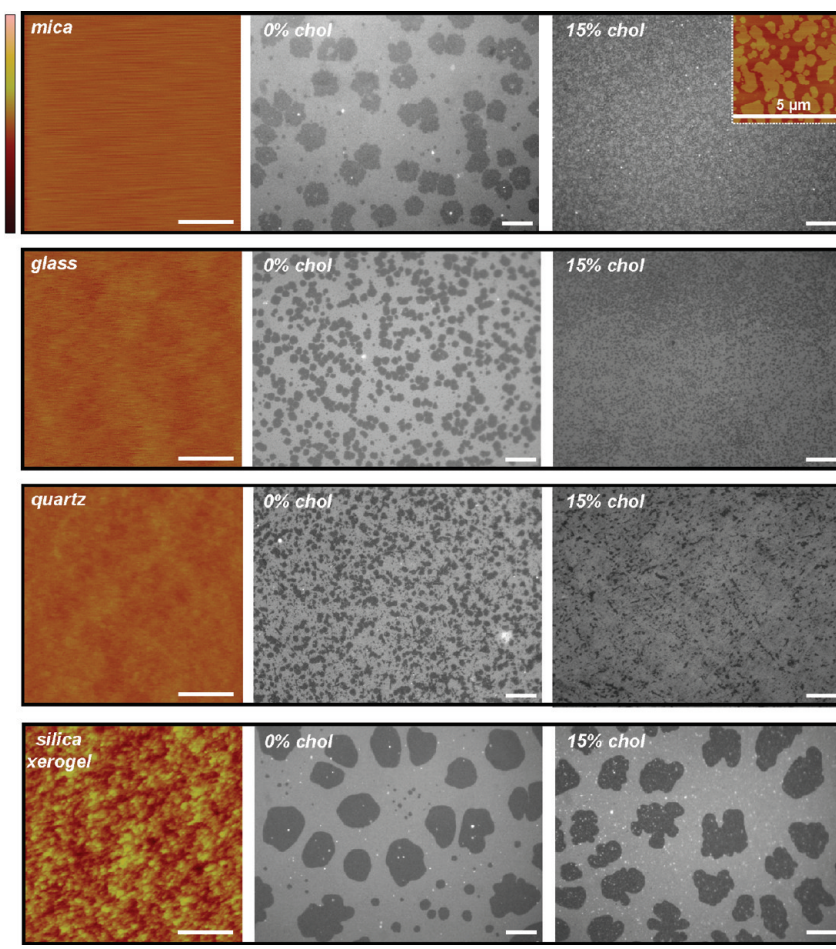


Figure 5. Influence of surface curvature versus surface chemistry on the domain properties in DOPC/DSPC (1/1 mole ratio)/chol-supported lipid bilayers. (Left) AFM images showing that the surface roughness of mica, glass, and quartz are similar to each other while the silica xerogel surface is rougher. (Middle and right) Fluorescence (and AFM, inset) images showing that the addition of 15 mol % chol resulted in a decrease in domain size for mica-, glass-, and quartz-supported lipid bilayers whereas the domain size did not decrease for silica xerogel-supported lipid bilayers. Scale bars on AFM images on the left and fluorescence images represent 500 nm and 15 μm , respectively. Color bar on the upper left corner represents 10 nm. Cooling rates for mica-, glass-, quartz-, and silica xerogel-supported lipid bilayers were 10, 5, 5, and 20 $^{\circ}\text{C}/\text{h}$, respectively.

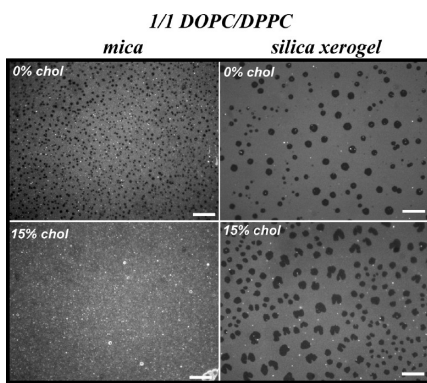


Figure 6. Fluorescence microscopy images of DOPC/DPPC (1/1 mole ratio)/(0 and 15 mol % chol) bilayers supported by (left) mica and (right) silica xerogel substrates. Domain sizes are decreased more effectively by the addition of chol on the mica surface compared to the silica xerogel surface. Scale bars represent 15 μm . Cooling rate was 20 $^{\circ}\text{C}/\text{h}$.

DLPC/DSPC/chol bilayers prepared at a mixture chol concentration above the known miscibility point of ~ 20 mol % chol.²⁸

There were some subtle differences in the characteristics of the mixtures compared to the DOPC/DSPC/chol mixtures due to the

variations in the nature of the lipids. DPPC (16 carbons) has less carbons in its tails as compared to DSPC (18 carbons). This resulted in smaller domains as can be observed by comparing Figure 6 (silica xerogel, 0 mol % chol) to Figure 2 (X1) because of the smaller hydrophobic mismatch with DOPC and corresponding lower line tension leading to increased number of nuclei, according to the classical nucleation theory.²⁹ As for DLPC/DSPC/chol, the miscibility point of 1/1 mol ratio DLPC/DSPC occurs at ~ 20 mol % chol which is lower than that of 1/1 mol ratio DOPC/DSPC (~ 40 mol % chol). Therefore, the disappearance of domains at 25 mol % on mica as shown in Figure 7 (mica, 25 mol % chol) represents the miscibility point.

For the DLPC/DSPC system, we quantified on the right side of Figure 7 domain area fraction, shape factor S , and domain size by analyzing fluorescence microscopy images up to 15 and 30 mol % chol for mica and silica xerogel substrates, respectively. On the mica substrate, as the chol concentration was increased to 15 mol %, the domain area fraction increased from 0.33 to 0.57 whereas domain size decreased substantially and S decreased slightly. On the silica xerogel substrate, as the chol concentration was

(28) Zhao, J.; Wu, J.; Shao, H. L.; Kong, F.; Jain, N.; Hunt, G.; Feigenson, G. *Biochim. Biophys. Acta, Biomembr.* **2007**, *1768*, 2777–2786.

(29) Blanchette, C. D.; Lin, W. C.; Orme, C. A.; Ratto, T. V.; Longo, M. L. *Langmuir* **2007**, *23*, 5875–5877.

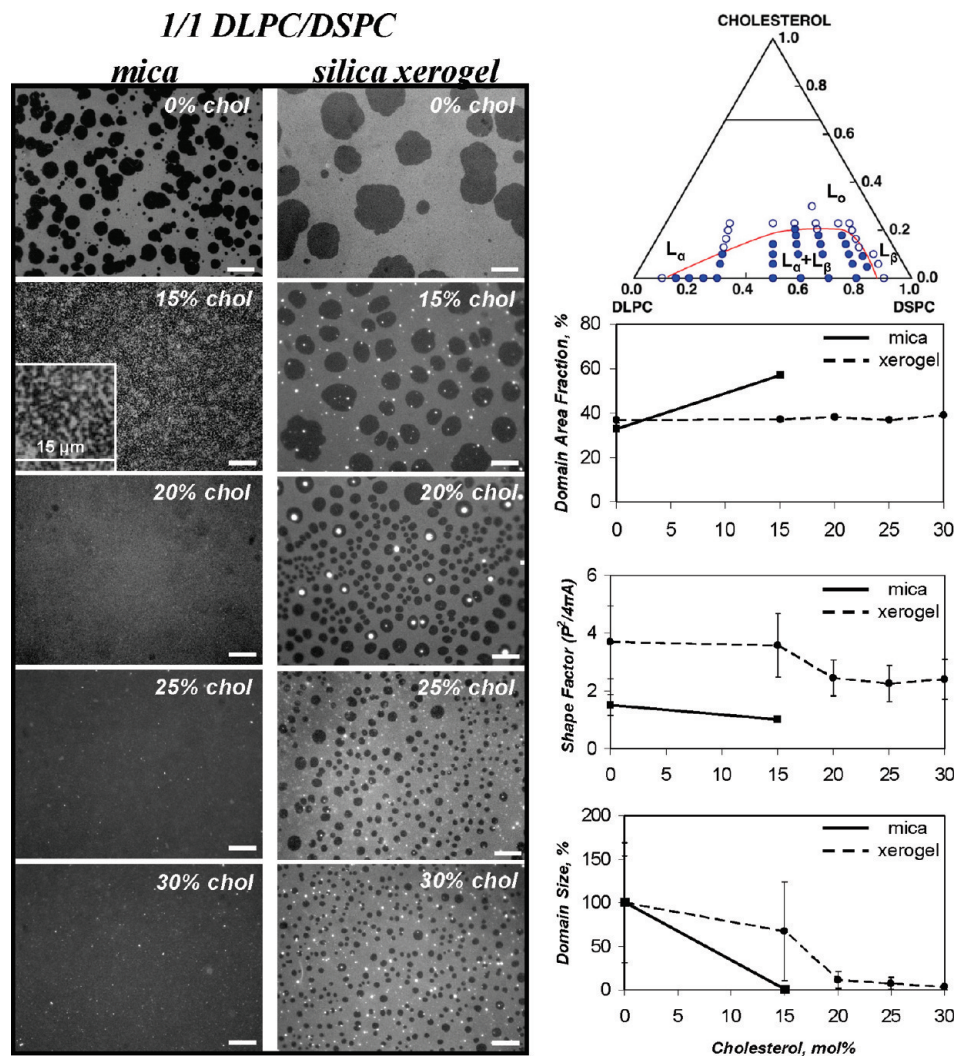


Figure 7. Fluorescence microscopy images of DLPC/DSPC (1/1/ mole ratio)/(0 and 15 mol % chol) bilayers supported by (left) mica and (middle) silica xerogel substrates. Domain sizes are decreased more effectively by the addition of chol on the mica surface compared to the silica xerogel surface. Domains on silica xerogel persist through 30 mol % chol in disagreement with the ternary phase diagram for GUVs (top right), inferring a difference in composition and/or phase diagram on this high curvature/roughness surface. (Right) Domain area fraction, shape factor, and domain size for mica-supported (solid lines) and silica xerogel-supported (dashed lines) lipid bilayers versus chol concentration of vesicles used in preparation (cooling rate of 20 °C/h). The domain area fraction is given in percent. The domain sizes are given in terms of % values with respect to 0 mol % chol results. Error bars represent one standard deviation. No error bars are present for domain area fraction, since the data were obtained using all images for each substrate. Scale bars represent 15 μm. Ternary phase diagram reprinted from ref 28 with permission from Elsevier. Phase notation from Marsh²¹ has been added.

increased, the domain area fraction was constant at ~0.37 and only increased slightly to 0.39 at 30 mol % chol. Decreases in domain size and S that occurred at 15 mol % chol for the mica substrate occur at 30 and 20 mol %, respectively, for the silica xerogel substrate. To sum up, when we changed the chain length and degree of unsaturation of the gel and lipid components, respectively, we continued to observe shifts to higher mol % chol for miscibility and changes in domain area fraction, S , and domain size for the silica xerogel substrate compared to the mica substrate as previously observed in Figure 4.

Discussion

Phase Behavior and Composition in Mica-Supported Lipid Bilayers Agree with those of GUVs. We found that the phase separation of mica-supported DOPC/DSPC (1/1 mol/mol)/chol bilayers quantitatively agreed with the phase diagram (Figure 1) that had been previously obtained from GUV data by Zhao et al.²² Importantly, the domain area fraction results on

mica were almost identical to those calculated from the phase diagram using the lever rule and molecular areas. Therefore, the supported lipid bilayer compositions were the same as the vesicles used to make them and the tie lines were comparable to the phase diagram. The miscibility composition observed in the mica-supported lipid bilayers was in very good agreement with the upper boundary of the L_a+L_o region once uncertainties in the GUV phase diagram were taken into account. Specifically, there was a slight shift to a higher value on mica-supported lipid bilayers (miscibility was between 40 and 50 mol % chol compared to 38 mol % chol on the phase diagram). However, in the GUV study used to obtain the phase diagram, it was noted that the unusual flatness of the upper boundary of the L_a+L_o region could be attributed to the possibility of the presence of coexisting domains that are too small to detect by fluorescence microscopy at this region.²² Indeed, using AFM imaging, we were able to detect submicrometer-scale domains still existing at 40 mol %. In ternary phase diagrams, the upper boundary of the L_a+L_o region

should closely parallel the slope of the nearest three-phase line.²¹ Taken together, the upper boundary of the $L_{\alpha}+L_o$ region in Figure 1 should have a slight upward (left to right) slope probably parallel to the three-phase $L_{\alpha}+L_o+L_{\beta}$ tie line that lies below it.

The only significant difference observed in the phase behavior of mica-supported lipid bilayers compared to the phase diagram obtained by GUVs²² is the shift of the lower phase boundary of the three-phase $L_{\alpha}+L_o+L_{\beta}$ region. We could observe three-phase coexistence at 5 mol % chol, whereas the three-phase coexistence region in the phase diagram given in Figure 1 starts at ~12 mol % chol for 1/1 mol ratio DOPC/DSPC mixtures. Our result at 5 mol % chol would, however, be in much better agreement with the phase diagram of Figure 1, if the lower phase boundary of the three-phase $L_{\alpha}+L_o+L_{\beta}$ region were flat rather than sloping upward from left to right. Indeed, for ternary phase diagrams, each side of a three-phase triangle must be almost parallel to the closest tie line in its adjacent two-phase region²¹ which in this case is the flat 0 mol % chol base of the ternary phase diagram. A flat lower phase boundary of the three-phase $L_{\alpha}+L_o+L_{\beta}$ region at ~5 mol % would correlate well with the L_{β} to L_o+L_{β} transition for DSPC/chol found by Almeida et al. to occur at ~5 mol % chol.³⁰ We detected the three-phase coexistence differently, by qualitative fluorescence imaging of the partitioning of the very small fluorescent probe, NBD-PC, in comparison to the methods used by Zhao et al.²² that extensively used bulkier DiI type dyes, possibly accounting for the difference in phase behavior.

We account for such excellent quantitative agreement in phase separation to the similarities in thermal history of our mica-supported lipid bilayers and the GUVs²² of the previous study. Both supported lipid bilayers and GUVs are cooled slowly from above the T_m of the gel species to 23 °C over a period of several hours. For domains, slow cooling promotes a slow nucleation rate and slow growth rate (reaction limited conditions), and affords time for edge diffusion, Ostwald ripening, and coalescence, all rate processes that move the system toward equilibrium.²⁷ In supported lipid bilayers, coalescence is mainly restricted to domains that grow into contact, making it a slower process in supported lipid bilayers compared to GUVs. Similar rates and time scales for these processes in both mica-supported and GUV systems yield supported lipid bilayers with tractable and similar phase behavior as we have demonstrated in the past.^{31,32} By contrast, supported lipid bilayers that have been prepared with a significantly different thermal history in comparison to GUVs have been shown to display significantly different phase behavior.^{22,33} Specifically, supported lipid bilayers have been prepared from vesicles deposited at 23 °C with no subsequent thermal step^{22,33} to drive the lipid bilayer toward equilibrium as typically is used in GUVs as the last step of preparation. It also should be noted that, in the preparation of both supported lipid bilayers and GUVs, the lipids at one stage are dried from a solvent-spread film. Recently, Buboltz et al.³⁴ have shown evidence that the drying stage induces long-lived demixing and that small vesicles prepared without such a drying step have a much smaller $L_{\alpha}+L_o$ region in a ternary phase diagram and much higher chol solubility. Therefore, although GUVs and supported lipid bilayers can be driven similarly toward equilibrium by the use of a thermal cooling step, equilibrium may

not be possible with the drying step currently used for sample preparation.

Trends As Expected in Area Fraction, Shape Factor, and Size in Supported Lipid Bilayers. The trends for DOPC/DSPC(1/1 mol/mol)/chol bilayers in domain area fraction, shape factor S , and domain size can be explained by the phase diagram in Figure 1 and the relationship between the various phases and their physical properties. As calculated in the Results section, the trend in increasing area fraction with increasing chol concentration is in agreement with the 0 mol % chol tie line and the tie line corresponding to the upper phase boundary of the three-phase $L_{\alpha}+L_o+L_{\beta}$ region. The initial decreasing trend in S as the chol concentration is increased represents a rounding of the domains resulting from a conversion of the domain phase to a more fluid semicrystalline phase, and it has been observed commonly in GUVs with similar phase behavior.^{22,35,36} It has been shown that domains in GUVs remain rounded and grow large through coalescence as the chol concentration is further increased.^{22,35,36} By addition of chol, the domains in this study are visually seen to coalesce by merging with each other, but because the domains are pinned to the substrate, they do not coalesce into large rounded domains. Thus, the S value increased in this study as the domains took on a more networked appearance.

Finally, the trend of decreasing domain size with increasing chol is expected for pinned domains, where because of slow coarsening dynamics the domain size reflects the nucleation rate corresponding exponentially to the negative of domain line tension by classical theory of nucleation.^{29,37} As chol concentration is increased, the phases become more mixed as is evident by examining the narrowing of the coexistence regime as one moves up the phase diagram toward 100 mol % chol in Figure 1. Thus, the line tension is lowered^{37,38} as the height mismatch and mechanical properties of the phases present begin to merge (i.e., line tension becomes zero at the critical point). According to the classical theory of nucleation, an increase in line tension, area per molecule, or a decrease in the enthalpy of the DSPC-rich phase may have accounted for the larger area of domains supported by the high curvature silica xerogel in comparison to mica, when the same thermal cooling rate was used. The plausible increase in area per molecule in the high curvature silica xerogel environment will be discussed below with respect to the work of Brumm et al.¹¹ We observe a 3.5× increase in average domain size for silica xerogel-supported lipid bilayers with the addition of 5 mol % chol. Scrutiny of the images and domain size statistics reveals that the increase is likely caused by Ostwald ripening as a population of small domains disappears between 0 and 5 mol % chol and the average domain size increases. It is not surprising that Ostwald ripening is a significant mechanism for domain growth at low (but not zero) chol concentration as a result of a high line tension (the driving force for Ostwald ripening) and increased fluidity of DSPC.

The trends are similar in the DLPC/DSPC/Chol system despite the fact that only $L_{\alpha}+L_{\beta}$ coexistence is present in the enclosed region of the phase diagram. The similarity reflects the fact that the domain and surrounding lipids are becoming more mixed in both systems as chol is added and that the left boundary of the $L_{\alpha}+L_{\beta}$ phase (red line of phase diagram in Figure 7) slopes

(30) Almeida, P. F. F.; Vaz, W. L. C.; Thompson, T. E. *Biophys. J.* **1993**, *64*, 399–412.

(31) Lin, W. C.; Blanchette, C. D.; Longo, M. L. *Biophys. J.* **2007**, *92*, 2831–2841.

(32) Blanchette, C. D.; Lin, W. C.; Ratto, T. V.; Longo, M. L. *Biophys. J.* **2006**, *90*, 4466–4478.

(33) Stottrup, B. L.; Veatch, S. L.; Keller, S. L. *Biophys. J.* **2004**, *86*, 2942–2950.

(34) Buboltz, J. T.; Bwalya, C.; Williams, K.; Schutze, M. *Langmuir* **2007**, *23*, 11968–11971.

(35) Veatch, S. L.; Keller, S. L. *Phys. Rev. Lett.* **2005**, *94*, 4.

(36) Bjorkqvist, Y. J. E.; Brewer, J.; Bagatolli, L. A.; Slotte, J. P.; Westerlund, B. *Biochim. Biophys. Acta, Biomembr.* **2009**, *1788*, 1310–1320.

(37) Blanchette, C. D.; Lin, W. C.; Orme, C. A.; Ratto, T. V.; Longo, M. L. *Biophys. J.* **2008**, *94*, 2691–2697.

(38) Tian, A. W.; Johnson, C.; Wang, W.; Baumgart, T. *Phys. Rev. Lett.* **2007**, *98*, 4.

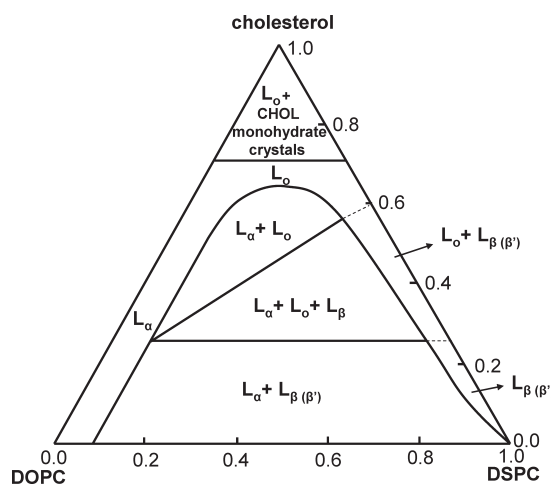


Figure 8. Proposed ternary phase diagram for silica xerogel-supported DOPC/DSPC/chol bilayer at 23 °C based upon data in ref 22 and our experimental results. The silica xerogel surface presents a matrix of 50 nm silica beads with a surface roughness of ~1 nm.

upward from left to right similar to the upper boundary of the three-phase region in Figure 1.

Therefore, the trend lines of domain area fraction, S , and domain size versus chol concentration are as expected according to the phase diagrams and known phase behavior. However, the use of a high curvature silica xerogel substrate compared to a flat substrate (such as mica, glass, or quartz) stretches the trend lines to higher chol concentration as was quantified in Figures 4 and 7.

Curvature Controlling Composition or Demixing of Silica Xerogel-Supported Lipid Bilayers. The stretching of trend lines of domain area fraction, S , and domain size versus chol concentration and miscibility to higher chol concentration can be explained either by a discrepancy in the chol concentration or by a change in the phase diagram (Figure 1) of the silica-supported DOPC/DSPC (1/1 mol ratio)/chol lipid bilayers. A significantly lower chol concentration in the supported lipid bilayer in comparison to the SUVs used to form the supported lipid bilayer while maintaining the same phase diagram would explain the results. Alternatively, the results can be explained by an altered phase diagram where the coexistence region has essentially been stretched toward the 100 mol % chol vertex for the DOPC/DSPC/chol bilayer on the high curvature silica xerogel surface (Figure 8). In the second case, the supported lipid bilayer and SUV compositions are identical. There is evidence in the literature for these mechanisms arising from curvature-controlled intramembrane transport of chol or curvature-induced lateral demixing. It is possible that both mechanisms are taking place.

Chol is known to be able to move spontaneously between biomembranes.^{39–43} There is strong evidence in the literature that proposes a mechanism via an aqueous diffusion pathway in which chol diffuses through the medium that separates donor and acceptor vesicles.^{39,40,43} The curvature of the vesicles from which desorption occurs directly affects the rate of chol efflux; that is, higher rates were observed for smaller donor vesicles compared to larger donor vesicles.^{8–10} This was attributed to the looser packing of the lipid molecules in a high curvature configuration

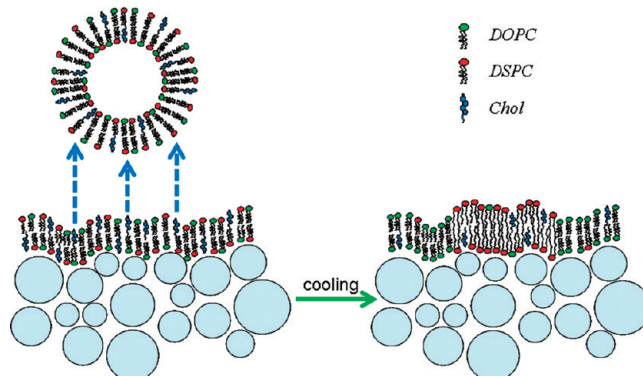


Figure 9. Schematic representation of (left) proposed chol transfer from the high curvature silica xerogel-supported lipid bilayer to the lower curvature vesicles in the medium during the 65 °C vesicle fusion and incubation step. (Right) Consequently, the 23 °C lipid bilayer includes less chol than the composition of the vesicles used for supported lipid bilayer formation.

enhancing the chol efflux. Indeed, it has been recently shown that an increase in surface curvature causes extensive broadening of gel to liquid-crystalline phase transition⁴⁴ which is known to reflect looser packing of the lipids.⁴⁵ In a previous study, the half-times of desorption at room temperature of chol from 46 ± 17 nm and 181 ± 43 nm diameter PC vesicles were calculated to be 1.76 ± 0.03 h and 9.43 ± 0.36 h, respectively.¹⁰ Additionally, in a population containing aggregates differing greatly in curvature, namely, micelles and small unilamellar vesicles, chol to phospholipid ratios are significantly lower by about one-quarter in the higher curvature micelles compared to SUVs.⁴⁶

Invoking the mechanism of chol partitioning between lipid bilayer phases of various curvature and the water phase, we recognize that the silica xerogel-supported lipid bilayers were formed by vesicle fusion at 65 °C and then incubated with vesicles for several hours, while cooling, followed by a rinsing step with water. The average bead size of the silica xerogel structure used in our experiments measured by AFM was 50 ± 21 nm in diameter, whereas the average size of the vesicles was 167 ± 49 nm in diameter (measured by particle sizer after cooling in an identical fashion to the supported lipid bilayers). It was previously reported that the domain nucleation temperature of 3:2 mol ratio DOPC/DSPC mixture on mica was 44 ± 0.5 °C.²⁷ If we roughly assume a close nucleation temperature on silica xerogel, then there would be ~1 h time interval before the nucleation occurs. This time would be sufficient for a considerable amount of chol transfer from the higher curvature supported lipid bilayer to the vesicles in the medium, as the half-time at 23 °C is 1.76 ± 0.03 h and this half-time would be decreased at the higher temperature. In this mechanism, domains would form after the majority of this compositional equilibration took place, and therefore, nanometer-scale corrugations could regulate the composition of domains of much larger size. The cartoon in Figure 9 summarizes this proposed mechanism for the observations. This mechanism suggests that our silica xerogel-supported lipid bilayers simply contained a lowered amount of chol in comparison to the SUVs used in the vesicle fusion step and that the ternary phase diagram

- (39) McLean, L. R.; Phillips, M. C. *Biochemistry* 1981, 20, 2893–2900.
- (40) Backer, J. M.; Dawidowicz, E. A. *Biochemistry* 1981, 20, 3805–3810.
- (41) Thomas, P. D.; Poznansky, M. J. *Biochem. J.* 1988, 251, 55–61.
- (42) Toledo, J. D.; Tricerri, M. A.; Corsico, B.; Garda, H. A. *Arch. Biochem. Biophys.* 2000, 380, 63–70.
- (43) McLean, L. R.; Phillips, M. C. *Biochemistry* 1982, 21, 4053–4059.

(44) Mitomo, H.; Chen, W. H.; Regen, S. L. *Langmuir* 2009, 25, 4328–4330.

(45) Mabrey-Gaud, S. From Physical Structure to Therapeutic Applications. In *Liposomes*; Knight, C. G., Ed.; Elsevier/North-Holland Biomedical Press: New York, 1981.

(46) Moschetta, A.; Eckhardt, E. R. M.; De Smet, M. B. M.; Renooij, W.; Van Berge-Henegouwen, G. P.; Van Erpecum, K. J. *Biochim. Biophys. Acta, Mol. Cell Biol. Lipids* 2001, 1532, 15–27.

for the silica xerogel-supported lipid bilayers is not necessarily altered significantly from that in Figure 1.

Brumm et al.¹¹ examined curvature induced demixing in binary DMPC/DSPC bilayers adsorbed to 640 ± 40 nm and 60 ± 6 nm silica beads by differential scanning calorimetry and Fourier transform infrared spectroscopy. They explained their results of increasing demixing of DMPC and DSPC as the curvature increased by using regular solution theory. In their explanation, the lowered lateral pressure induced by high curvature exerts a higher energy penalty than the bending energy. This energy penalty is felt most strongly by the gel-phase lipids that are packed closely together, and therefore, an increase in their area per molecule in a curved environment will drastically change the free energy of the lipid bilayer. The theory's prediction that the two components will demix further as the curvature increases agrees with their data showing a significantly narrowing of the DSPC phase transition and a downward shift in temperature of the DMPC phase transition. More recently, demixing studied in ternary systems containing chol, similar to ours, have been carried out using lipid bilayer tubules of decreasing radius pulled from GUVs.^{47,48} These studies also demonstrate that high curvature promotes lipid demixing, and in these cases this was detected essentially by increases in the critical mixing/demixing chol concentration of the ternary phase diagram. In the case of Tian et al.'s study,⁴⁸ lipid spontaneous curvature and bending stiffness were invoked as the main driving forces for lipid demixing. This argument should be applicable to a corrugated surface because positive and negative curvature values are squared when determining the bending energy and therefore they will not cancel out.⁴⁹

Invoking the mechanism of increased lipid demixing to our (DLPC or DOPC)/(DSPC, DPPC, or DiC15PC)/chol system, we recognize that the energy penalty of curvature will be greatest with respect to the gel-phase component as pointed out by Brumm et al. In the ternary phase diagram, stretching the coexistence region toward 100% chol as shown in Figure 8 for DOPC/DSPC/chol would limit mixing of DOPC into the DSPC-rich phase as the chol concentration is increased. Through demixing, the increase in the area per molecule of the DSPC lipids is limited in the highly corrugated surface of the micrometer-scale domain. This new phase diagram would explain the stretching to higher chol concentration for the trend lines observed here. For example, comparing Figure 8 to Figure 1, the characteristics of silica-supported lipid bilayers at approximately 40 mol % chol should be similar to the characteristics at 15 mol % chol for GUVs and mica-supported lipid bilayers. To our knowledge, such large-scale demixing induced by curvature has not been observed before, as the previous systems utilized individual nanometer-scale silica beads and single tubules of 10 nm scale radius. Such large-scale demixing, that is, at the scale of the plasma membrane, induced by surface roughness is particularly applicable to study the impact of cell membrane topology on membrane phase behavior. An interesting implication of this new phase diagram is that increasing curvature and lowering temperature have the same impact on the $L_o + L_\beta$ to L_o transition; that is, this transition is shifted to higher chol concentration. For example, according to Marsh,²¹ a decrease in temperature from 23 to 10 °C necessarily shifts this transition for DPPC bilayers from ~30 mol % chol to

approximately to 70 mol % chol, based upon the ternary phase diagrams for DOPC/DPPC/chol GUVs obtained by Gawrisch and co-workers.⁵⁰ To our knowledge, the impact of curvature on the $L_o + L_\beta$ to L_o transition has not been investigated.

Conclusions and Future Work

Here we used fluorescence microscopy and atomic force microscopy to characterize ternary lipid bilayers supported by mica, silica xerogel, borosilicate glass, and quartz. The primary ternary composition that we examined was DOPC/DSPC (1/1 mol ratio)/cholesterol for comparison to the GUV phase diagram of Zhao et al.²² We found that, on the mica support, the DSPC-rich domain area fractions and phase transition compositions were in very good agreement with the phase diagram of Zhao et al.²² A similar thermal history of our mica-supported lipid bilayers and GUVs accounted for the agreement. Domain area fraction, shape factor (S), and domain size were quantitatively characterized by image analysis for comparison of mica-supported to silica xerogel-supported ternary mixtures. It was found that both mica-supported and silica xerogel-supported lipid bilayers followed similar trends in these characteristics with increasing cholesterol that could be explained based upon phase behavior of ternary lipid mixtures. For example, domain size decreased as cholesterol concentration increased as predicted by the decreasing line tension accompanying mixing. However, these trend lines were quantitatively stretched to higher cholesterol concentration on the silica xerogel substrate versus the mica substrate. We implicated high curvature rather than surface chemistry as responsible for these shifts in the trend lines by comparing images of DOPC/DSPC/cholesterol bilayers supported on high curvature (0.04 nm^{-1})/roughness (~1 nm) silica xerogel, mica (smooth and most different surface chemistry), quartz (smooth and same surface chemistry), and borosilicate glass (smooth and different surface chemistry). Ternary mixtures with slightly shorter chain lengths of the gel-phase component or a saturated fluid-phase component still gave significant shifts to higher cholesterol concentration in these characteristics with the use of the silica xerogel substrate.

We hypothesized that shifts in the trend lines of the ternary lipid bilayers to higher cholesterol concentration in the high curvature environment of the silica xerogel could be caused by two mechanisms that are both supported by literature. In the first mechanism, cholesterol transferred from the higher curvature supported lipid bilayer to the vesicles in the medium during the vesicle fusion and thermal cooling step. The transfer resulted in a significantly lower cholesterol concentration in the supported lipid bilayer in comparison to the SUVs used to form the supported lipid bilayer. In the second mechanism, high curvature promotes sustained lipid demixing, particularly of the fluid- and gel-phase components. Thus, in a high curvature environment, a new phase diagram must be invoked which stretches the coexistence region toward 100% cholesterol in comparison to the phase diagram for the flat environment.

It should be possible to determine which of these two mechanisms is dominant, and this will be the focus of future work. The first mechanism infers that cholesterol content of a supported lipid bilayer with high curvature corrugation is dependent upon the supported lipid bilayer formation and equilibration method and therefore different methods should give different results. For example, using smaller SUVs to form the supported lipid bilayers should result in a higher content of cholesterol compared to the

(47) Sorre, B.; Callan-Jones, A.; Manneville, J. B.; Nassoy, P.; Joanny, J. F.; Prost, J.; Goud, B.; Bassereau, P. *Proc. Natl. Acad. Sci. U.S.A.* **2009**, *106*, 5622–5626.

(48) Tian, A. W.; Capraro, B. R.; Esposito, C.; Baumgart, T. *Biophys. J.* **2009**, *97*, 1636–1646.

(49) Rozycski, B.; Weikl, T. R.; Lipowsky, R. *Phys. Rev. Lett.* **2008**, *100*, 4.

(50) Veatch, S. L.; Soubias, O.; Keller, S. L.; Gawrisch, K. *Proc. Natl. Acad. Sci. U.S.A.* **2007**, *104*, 17650–17655.

use of larger SUVs. Variations in incubation times with the SUVs or a completely different supported lipid bilayer deposition technique, for example, spin-coating,⁵¹ should also significantly alter the transport and intrabilayer and lipid-bilayer–aqueous partitioning of cholesterol. The second mechanism infers that for a supported lipid bilayer with high curvature corrugation there should be enhanced demixing of the two PC lipid components and therefore this enhanced demixing should be detectable by the use of binary lipid mixtures, thus eliminating the possible first competing mechanism. Rather than the nearly immiscible PC lipids chosen here, the second mechanism should be tested by using binary lipid mixtures where mixture behavior in a flat

environment deviates slightly from ideal mixing (in comparison to DOPC/DSPC or DLPC/DSPC), and therefore further deviations (demixing) from ideality could be detected in a supported lipid bilayer with high curvature corrugation. For example, composition/temperature phase diagrams of closer chain-matched DMPC/DSPC or DLPC/DPPC silica xerogel-supported lipid bilayers could be generated using area fraction measurements (as generated here) and compared to the same lipid bilayers on mica supports and the literature.⁵² Finally, more well-defined membrane corrugations, in comparison to the silica xerogel surface, may be generated through the use of nanofabrication techniques, such as electron beam lithography, to form substrates.

(51) Bernchou, U.; Ipsen, J. H.; Simonsen, A. C. *J. Phys. Chem. B* **2009**, *113*, 7170–7177.

(52) Mabrey, S.; Sturtevant, J. M. *Proc. Natl. Acad. Sci. U.S.A.* **1976**, *73*, 3862–3866.

Acknowledgment. We acknowledge funding by the NSF NIRT Program (CBET 0506602) and the NSF MRSEC Program CPIMA (NSF DMR 0213618).